Flexibility of telomerase in binding the RNA template and DNA telomeric repeat

Woo Suk Choi[a], Peter J. Weng[a,1], and Wei Yang[a,2]

[a]Laboratory of Molecular Biology, National Institute of Diabetes and Digestive and Kidney Diseases, NIH, Bethesda, MD 20892

Contributed by Wei Yang; received September 1, 2021; accepted November 22, 2021; reviewed by Feng Qiao and Y. Whitney Yin

Telomerase synthesizes telomeres at the ends of linear chromosomes by repeated reverse transcription from a short RNA template. Crystal structures of *Tribolium castaneum* telomerase reverse transcriptase (*tc*TERT) and cryoelectron microscopy (cryo-EM) structures of human and *Tetrahymena* telomerase have revealed conserved features in the reverse-transcriptase domain, including a cavity near the DNA 3′ end and snug interactions with the RNA template. For the RNA template to translocate, it needs to be unpaired and separated from the DNA product. Here we investigate the potential of the structural cavity to accommodate a looped-out DNA bulge and enable the separation of the RNA/DNA hybrid. Using *tc*TERT as a model system, we show that a looped-out telomeric repeat in the DNA primer can be accommodated and extended by *tc*TERT but not by retroviral reverse transcriptase. Mutations that reduce the cavity size reduce the ability of *tc*TERT to extend the looped-out DNA substrate. In agreement with cryo-EM structures of telomerases, we find that *tc*TERT requires a minimum of 4 bp between the RNA template and DNA primer for efficient DNA synthesis. We also have determined the ternary-complex structure of *tc*TERT including a downstream RNA/DNA hybrid at 2.0-Å resolution and shown that a downstream RNA duplex, equivalent to the 5′ template-boundary element in telomerase RNA, enhances the efficiency of telomere synthesis by *tc*TERT. Although TERT has a preformed active site without the open-and-closed conformational changes, it contains cavities to accommodate looped-out RNA and DNA. The flexible RNA–DNA binding likely underlies the processivity of telomeric repeat addition.

DNA loopout | cavity | telomeric repeat synthesis | template-boundary element | RNA-template translocation

In most eukaryotic cells, telomeres made of G-rich repeats cap and protect the ends of linear chromosomes from degradation, fusion, and shortening (1). Telomerase, which synthesizes telomeric DNA repeats, is composed of two essential components, telomerase reverse transcriptase (TERT) and telomerase RNA (TER), along with a battery of cofactors (2–4). TERT harbors the catalytic activity and copies the telomeric RNA-template sequence embedded in TER into DNA repeats (5, 6). Each chromosome end contains tens to hundreds of telomeric DNA repeats of 5 to 8 nt (http://telomerase.asu.edu/sequences_tr.html). However, the telomere RNA template consists of only 1.5 to 1.8 repeats of the telomeric sequence. It is unclear how TERT uses the RNA template multiple times and adds telomeric repeats iteratively and often processively (7).

In each cycle of repeat addition, TERT synthesizes one telomere repeat and stops at the end of the template, which is marked by a 5′ template-boundary element (TBE) often consisting of a short duplex (Fig. 1*A*). Two different models have been proposed to account for the template RNA translocation. In the widely accepted model (6), the RNA template separates from telomeric DNA product, translocates by one repeat length, and reanneals with the DNA for the next round of repeat synthesis (Fig. 1*A*, steps 1 and 2). The process of RNA and DNA unpairing and rehybridization would be energetically costly. Interestingly, no helicase or energy input is required for telomere synthesis (6). Moreover, a prerequisite for the proposed model to work is sufficient space within TERT for the RNA and DNA to dissociate from each other, while remaining bound to TERT.

Alternatively, a looped-out DNA model proposes that the RNA-template translocation occurs in two steps and only a half of the RNA/DNA hybrid is separated in each step (8). At first, the telomeric DNA translocates with the template RNA by maintaining 2 bp upstream, while anchoring the 3′ end in the TERT active site (Fig. 1*B*). As a result, one telomeric repeat of DNA is extruded as a looped-out pseudohairpin (Fig. 1*B*, step 1). Before the next round of repeat synthesis, the looped-out DNA unfolds and reanneals with the RNA template (Fig. 1*B*, step 2). In this model, the looped-out DNA serves as an intermediate in RNA-template translocation and a stepping stone to partially preserve the hydrogen bonds between the RNA and DNA. However, this alternative model also requires space to accommodate the looped-out DNA and for DNA realignment.

Structures of *Tribolium castaneum* (red flour beetle) TERT (*tc*TERT) complexed with an RNA/DNA hybrid, and human and *Tetrahymena* telomerase including accessory subunits and telomeric DNA, have been reported (3, 4, 9). As the protein sequence and early structural analyses indicate (10, 11), the reverse-transcriptase domain (RT; composed of the finger and palm) and the ensuing C-terminal extension (CTE; equivalent to the thumb of RT) are superimposable among these TERTs.

Significance

Telomerase reverse transcriptase (TERT) has a conserved central cavity near the active site. Using enzymatic and mutagenesis analyses, we provide experimental evidence that an artificially looped-out telomeric repeat in the DNA primer can be transiently accommodated in the cavity of *Tribolium castaneum* (*tc*TERT). Kinetically, *tc*TERT requires a minimum of 4 bp between the RNA template and DNA primer for efficient DNA synthesis. An RNA duplex downstream of the RNA-template region after a flexible linker enhances the efficiency of primer extension by *tc*TERT. In addition to the peripheral cavities that accommodate looped-out RNA during each telomeric repeat synthesis, the central cavity that can accommodate the looped-out DNA may aid RNA-template translocation between cycles of telomeric repeat synthesis.

Author contributions: W.S.C., P.J.W., and W.Y. designed research; W.S.C. and P.J.W. performed research; W.S.C., P.J.W., and W.Y. analyzed data; and W.S.C., P.J.W., and W.Y. wrote the paper.

Reviewers: F.Q., University of California, Irvine; and W.Y.Y., The University of Texas Medical Branch at Galveston.

The authors declare no competing interest.

[1]Present address: Medical Scientist Training Program, Duke University School of Medicine, Durham, NC 27710.

[2]To whom correspondence may be addressed. Email: weiy@niddk.nih.gov.

This article contains supporting information online at http://www.pnas.org/lookup/suppl/doi:10.1073/pnas.2116159118/-/DCSupplemental.

Published December 30, 2021.

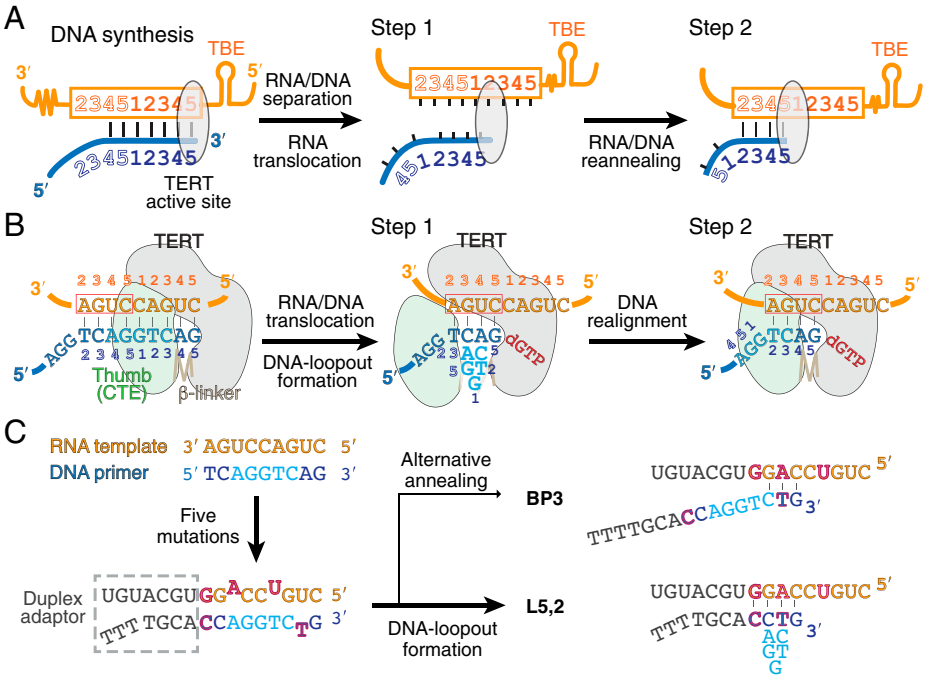

Fig. 1. Looped-out DNA model for repeat telomere synthesis. (*A*) The accepted model of RNA-template translocation and requirement of the hybrid separation. (*B*) The proposed DNA looped-out model with the *T. castaneum* telomeric sequence. (*C*) Design of a looped-out DNA primer (L5,2) based on the native telomere sequence and the possible alternative annealing, BP3. The mutated nucleotides in the RNA strand are highlighted in red and outlined in black, and those in the DNA strand are highlighted in purple and outlined in red.

The TER-binding domain (TRBD) N-terminal to RT has more sequence and structural variations than RTs (12–14). The TEN (telomerase essential N terminus) domain forms an appendage to the ring-shaped TERT core (RT, CTE, and TRBD) and binds the upstream TER and accessory subunits, which appear to stabilize the single-stranded DNA product (3, 4, 15) (*SI Appendix*, Fig. S1). *Tetrahymena* telomerase loses its catalytic activity without the TEN domain or with mutations disrupting its attachment to the TERT core (16). However, *tc*TERT, which naturally lacks a TEN domain, is active as a reverse transcriptase. Because TERs share little sequence conservation, the RNA component of telomerase has not yet been identified in insects, including red flour beetle. It is possible that a unique TER has coevolved with the TEN-less *tc*TERT. Because many beetles' telomeric repeat sequence is 5′-TCAGG-3′, which contains all four deoxyribonucleotides (17) and is not as G-rich as in vertebrates (5′-TTAGGG-3′), plants (5′-TTTAGGG-3′), and ciliates (5′-TTGGGG-3′), it may not require the TEN domain to untangle secondary structures formed in G-rich DNA.

The *tc*TERT and telomerase structures reveal an unusual but conserved central cavity between the palm and CTE domains, roughly 2 bp upstream from the DNA 3′ end (*SI Appendix*, Fig. S1*D*). The cavity is suggested to accommodate the looped-out DNA and allow the RNA/DNA hybrid to separate during RNA-template translocation (8). To test if the cavity can accommodate an extruded telomeric DNA repeat, we chose *tc*TERT as a model system because it is homologous to human and *Tetrahymena* TERT and was the only one with a crystal structure when we started this project. When macromolecular associations are too transient to be observed by NMR or X-ray crystallography, formation of reaction products can imply that a flexible substrate is captured transiently by the enzyme. Using enzymatic and mutagenic approaches, we show that *tc*TERT depends on the central cavity to accommodate and extend the looped-out DNA primer. We also find that a TBE-like RNA duplex downstream of the RNA template facilitates DNA synthesis. In contrast to HIV RT (18), TERT has a preformed active site, but bears multiple cavities that can accommodate looped-out RNA (*SI Appendix*, Fig. S1 *E* and *F*) and DNA.

Results and Discussion

Design of a Looped-Out Template/Primer Pair. To investigate whether *tc*TERT can bind a looped-out DNA, we prepared an RNA template and a DNA primer containing a looped-out telomeric repeat (Fig. 1*C*). Among the identified TERs, the RNA template often consists of a telomeric repeat (5 to 8 nt) plus 4 additional nucleotides and thus 1.5 to 1.8 telomeric repeats (6). In the animal and plant kingdom, the 5′ end of the RNA template is usually CU (encoding AG in the telomeric repeat) and occasionally CA as in ciliates, where telomeric DNA contains T and G only and no A (19). Thus, each telomeric repeat synthesis most often ends with a single G. Based on the telomeric sequence 5′-GTCAG-3′ (permutation of 5′-TCAGG-3′) of *T. castaneum* (17) and the conserved features of the RNA template, we designed a 9-nt (5 + 4 nt) template, 3′-AGUCCAGUC-5′ (Fig. 1*C*). To form a looped-out bulge exactly 2 nt upstream of the primer 3′ end containing the authentic telomeric sequence, which is 5′-AGGTC-3′ as dictated by the looped-out position (opposite 3′-UCCAG-5′; Fig. 1*B*) and to avoid formation of a perfect hybrid duplex by alternative annealing, we mutated two RNA and one complementary DNA bases downstream of the bulge (Fig. 1*C*). In addition, we replaced an A/T pair with a G/C pair upstream to stabilize the looped-out structure (Fig. 1*C*). The resulting hybrid of RNA template and DNA primer contained a 5-nt loopout flanked by 2 Watson–Crick base pairs on either side. An addition of 4 bp upstream was added to stabilize this RNA/DNA hybrid. Further upstream, 3 unpaired nucleotides on the template and primer each were included for potential interactions with *tc*TERT. The first C in the 5′ RNA overhang would direct dG incorporation if the looped-out DNA were bound by *tc*TERT. This substrate was named L5,2, denoting the 5-nt loopout and 2 bp after the extrusion (Fig. 1*C*).

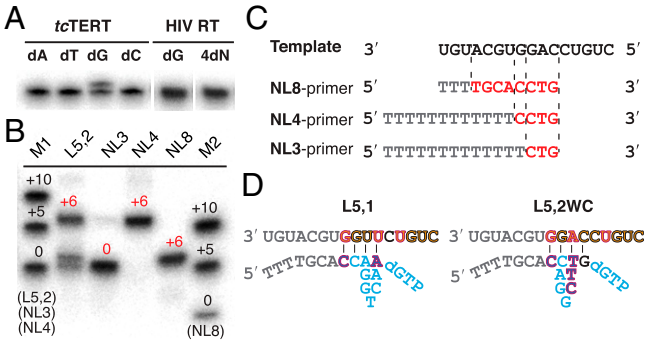

E

	k_{cat} (min^{-1})	K_M (μM)	K_{eff} ($min^{-1}μM^{-1}$)
L5,2	0.42 ± 0.01	443.9 ± 33.8	$0.95×10^{-3}$
NL8	18.5 ± 1.0	3.4 ± 0.5	5.47
NL4	0.67 ± 0.05	6.1 ± 1.0	0.11
NL3	$(0.83 ± 0.02)×10^{-2}$	431.4 ± 31.4	$0.19×10^{-4}$
L5,1	$(0.80 ± 0.03)×10^{-2}$	689.1 ± 67.3	$0.12×10^{-4}$
L5,2WC	$(9.7 ± 0.4)×10^{-2}$	461.7 ± 61.2	$0.21×10^{-3}$

Fig. 2. *tc*TERT extends various DNA primers including a loopout. (*A*) Nucleotide extension of L5,2 showed that *tc*TERT selectively incorporated dGTP opposite rC, but HIV RT failed to extend the L5,2 DNA primer with the loopout in the presence of dGTP or all four dNTPs. (*B*) In the presence of all four dNTPs and Mg^{2+}, *tc*TERT extended L5,2 to the end of the template with pausing after the first nucleotide incorporation. *tc*TERT extended NL4 and NL8 efficiently, but not NL3. Fuzzy weak bands of L5,2 and NL4 indicate possible additions of a second repeat. The lanes M1 and M2 contained +5 and +10 markers of L5,2 and NL8, respectively. (*C*) Substrate sequences of the RNA template and three variations of DNA primer, NL8, NL4, and NL3. Nucleotides in the primer strand that form base pairs with the template RNA are colored red. (*D*) Two variations of looped-out DNA primers. In L5,1 the looped-out position is shifted by 1 bp, and in L5,2WC, wobble base pairs in the loopout are replaced by Watson–Crick pairs. The mutated nucleotides in the RNA strand are highlighted in red and outlined in black, and those in the DNA strand are highlighted in purple and outlined in red. Positions of dNTP insertion (0) and the primer 3′ end (-1) are marked. (*E*) Summary of steady-state kinetic measurements of single-nucleotide primer extension of L5,2, NL8, NL4, NL3, L5,1, and L5,2WC by *tc*TERT.

***tc*TERT Can Extend the DNA Primer with a Looped-Out Bulge.** We found that *tc*TERT was able to extend L5,2 and selectively incorporate deoxyguanosine triphosphate (dGTP) (Fig. 2*A*). In contrast, a typical reverse transcriptase, HIV RT, failed to use L5,2 as a substrate for deoxyribonucleoside monophosphate (dNMP) incorporation (Fig. 2*A*). We investigated the processivity of L5,2 extension by *tc*TERT in the presence of all four deoxynucleoside triphosphates (dNTPs) and Mg^{2+}. *tc*TERT paused after incorporating deoxyguanosine monophosphate (dGMP) and then continued to the 5′ end of the RNA template (Fig. 2*B*). The 6-nt extension, 1 nt longer than the template, is probably due to the nontemplated addition often observed with DNA polymerase and reverse transcriptase (20, 21). A faint band at an ∼10-nt addition was also observed (Fig. 2*B*), indicating a repeat addition.

We checked alternative annealing between the RNA/DNA pair in L5,2, and found only one other possibility. A 3-bp hybrid (BP3) (Fig. 1*C*), if captured by *tc*TERT, might also result in the observed extensions (Fig. 2 *A* and *B*). To test whether *tc*TERT extends the 3-bp hybrid duplex, we synthesized a 3-bp hybrid (named NL3; NL, no loop) with the same RNA template but with a DNA oligo containing CTG at the 3′ end and otherwise all Ts to avoid unwanted secondary structures (Fig. 2*C*). With NL3, there was ∼50-fold less DNA extension product than with L5,2 under the same assay conditions (Fig. 2 *B* and *E* and *SI Appendix*, Fig. S2 *A* and *B*). We conclude that the product of the alternative annealing (NL3) is negligible, and the extensions observed (Fig. 2 *A* and *B*) are mainly from the looped-out DNA. The extension of L5,2 indicates that *tc*TERT must bind the looped-out bulge.

***tc*TERT Requires a Minimal 4-bp Primer for DNA Synthesis.** As the 3-bp hybrid (NL3) was not extended by *tc*TERT, we examined the minimal number of base pairs needed for *tc*TERT to effectively extend DNA. We extended the DNA unique sequence at the 3′ end to 5′-CCTG-3′ to form a 4-bp hybrid (NL4) for kinetic analysis (Fig. 2*C*). NL8, which contained the identical 8-bp hybrid as L5,2 but without the 5-nt loopout, was also made for comparison (Fig. 2*C*). Both NL4 and NL8 were extended well by *tc*TERT in the presence of all four dNTPs (Fig. 2*B*). However, NL8 was extended 51-fold more efficiently than NL4 (Fig. 2*E*). In comparison, L5,2 was extended 110-fold worse than that on NL4 because of a 74-fold increase of K_M, indicating very poor dGTP binding (Fig. 2*E*). The reduced binding of an incoming nucleotide is reminiscent of a mismatched DNA primer end (22). The low efficiency of L5,2 extension is expected based on the looped-out model, in which DNA looping out occurs transiently with the RNA-template translocation between cycles of telomeric repeat synthesis and is not meant to be extended (Fig. 1*B*).

The k_{cat} with NL3 was 50- to 80-fold lower than L5,2 and NL4, and the K_M with NL3 was similar to L5,2 and ∼70-fold higher than NL4 (Fig. 2*E*). It is surprising that changing from a 3-bp primer to 4 bp improves the catalytic efficiency of *tc*TERT ($K_{eff} = k_{cat}/K_M$) by 5,700-fold (see later sections for the structural explanation). The minimal requirement of 4 bp for *tc*TERT to efficiently extend the DNA primer correlates well with the RNA template consisting of 4 nt in addition to the telomeric repeat, which allows 4 bp between the RNA template and DNA primer at the beginning of each cycle of repeat addition (Fig. 1*A*). Coincidentally, the cryoelectron microscopy (cryo-EM) structures of *Tetrahymena* and human telomerase both show that a 4-bp hybrid of the RNA template and DNA is bound by TERT and, beyond the 4 bp, the RNA and DNA strands are separated by TERT even when they can form base pairs (4, 16).

Accommodation of the DNA Loopout Is Position- and Sequence-Dependent. The looped-out position of L5,2 was designed based on the location of the cavity relative to the RNA/DNA hybrid. However, the DNA looped-out position could shift by 1 nt if the nascent base pair between the RNA template and the incoming dGTP is counted as a part of the hybrid duplex. To determine whether the looped-out position is flexible, we synthesized L5,1 (Fig. 2*D*), in which the 5-nt loopout was shifted 1 bp closer to the primer 3′ end and the looped-out sequence became 5′-GGTCA-3′. The primer-extension rate on L5,1, however, was ∼50-fold lower than that with L5,2 (Fig. 2*E* and *SI Appendix*, Fig. S2*C*), indicating that the preferred position for a DNA loopout by *tc*TERT is between -2 and -3 from the replicating base pair.

We next examined whether the authentic telomeric sequence in the looped-out DNA is necessary for its accommodation. The single telomeric repeat sequence 5′-AGGTC-3′ may form 2 wobble base pairs (A/C and G/T) in the stem of a pseudohairpin (Fig. 1*B*). We altered 2 nt in the loop sequence (5′-AGGCT-3′, underlined) and thus replaced wobble base pairs with Watson–Crick pairs (A/T and G/C). The construct was named L5,2WC (Fig. 2*D*). While the K_Ms on L5,2WC and L5,2 were comparable, k_{cat} on L5,2WC was actually ∼5-fold lower than that on L5,2 (Fig. 2*E*). Although potentially forming perfect base pairs, the mutated sequence is worse in forming the looped-out

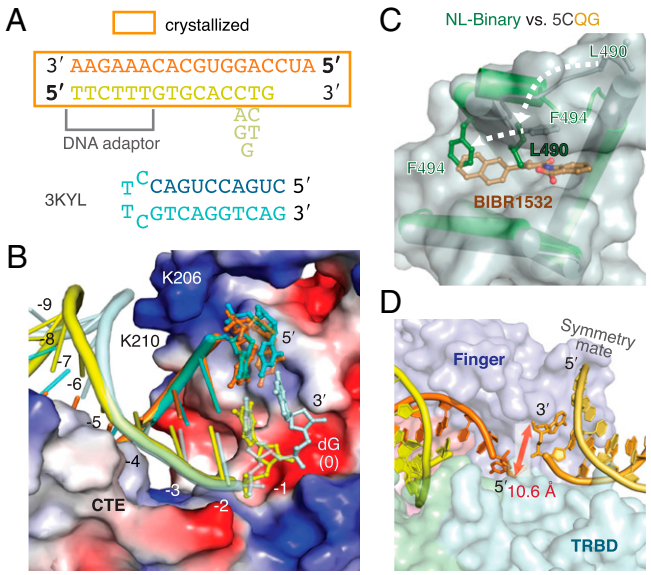

Fig. 3. Structure of the *tc*TERT–NL (RNA/DNA) binary complex. (*A*) Diagram of L5,2 and the NL RNA/DNA substrate used for crystallization with *tc*TERT. The RNA/DNA substrate sequence in 3KYL is shown (*Bottom*). (*B*) The NL binary complex structure is superimposed with 3KYL. The nucleic acids are color-coded as in Fig. 4*A*. The protein surface is shown with electrostatic potential, with blue representing positive charge and red representing negative charge. (*C*) A zoomed-in view of the blocked inhibitor-binding pocket. The NL binary-complex structure (shown in green) is superimposed with that of the inhibitor-bound *tc*TERT (PDB ID code 5CQG). Changes of 2 residues are indicated by dashed white arrows. (*D*) The crystal lattice contact made by two RNA/DNA molecules. The 5′ end of the RNA template and the 3′ end of its symmetry mate are juxtaposed in the same orientation (indicated by the red double arrowhead) and can be connected by 2 or 3 nt.

bulge or interacting with *tc*TERT. Taken together, these results suggest position- and sequence-dependent formation of the looped-out DNA.

Crystal Structure of a *tc*TERT–RNA/DNA Binary Complex. We tried to cocrystallize *tc*TERT with the looped-out DNA as well as normal hybrid (NL) substrates (Fig. 3*A*). Although looped-out substrates were not crystallized with *tc*TERT, a 15-bp NL duplex (Fig. 3*A*) produced crystals, which diffracted X-rays to 2.7-Å resolution. Mg^{2+} and dGMPNPP (a nonhydrolyzable dGTP analog) were included in the crystallization solution but not observed in the resulting structure, because of a metal chelator, citrate, in the buffer. When citrate was replaced by acetate, dGMPNPP and Mg^{2+} could be soaked into the active site (*SI Appendix*, Fig. S3*A*). The crystal structure of the NL binary complex (NL) was determined by molecular replacement based on the published *tc*TERT–RNA/DNA complex structure (Protein Data Bank [PDB] ID code 3KYL) (9). The refined NL structure (*SI Appendix*, Table S1), which is a substrate complex with an empty active site, and 3KYL, a product complex with the primer 3′ end occupying the incoming nucleotide-binding site, are superimposable, including 5 bp of the RNA/DNA hybrid immediately upstream of the active site (-1 to -5) (Fig. 3*B*). The cavity next to the -2 and -3 DNA primer persists. Opposite the cavity, the protein interface with the RNA template from the replicating base (0 position) to 4 bp upstream (-4) is snug and hydrophobic with a positively charged rim surrounding it (Fig. 3*B*).

The NL structure, however, reveals a different conformation of the FVYL motif in CTE (amino acids [aa] 486 to 496), which excludes the binding of the telomerase inhibitor BIBR1532 (23). Instead of the extended conformation as observed in the apo (3DU6) (11), binary (3KYL) (9), and BIBR1532-bound complex (5CQG) (23) and the recently published *tc*TERT–RNA/DNA prereaction binary complex (6USO) (24), in the NL–*tc*TERT binary complex the stretch of T487 to N492 adopts an α-helical structure and blocks the inhibitor binding by occupying the hydrophobic cavity with L490 and F494 side chains (Fig. 3*C*). Interestingly, neither L490 nor F494 is conserved, and F494 is replaced by Asn in most TERTs, including human (23). We suspect that human and other TERTs without a hydrophobic equivalent of F494 may be more sensitive to BIBR1532 than *tc*TERT.

Most intriguingly, in the NL–*tc*TERT structure, each *tc*TERT molecule binds the second half of a symmetry-related duplex (a double-stranded [ds]DNA adaptor) between the TRBD and finger domain (Fig. 3*D*) in addition to the RNA/DNA hybrid in the canonical substrate-binding site. The 5′ end of the template RNA and the 3′ end of the symmetry mate that interacted with the same *tc*TERT are juxtaposed in the same polarity, and the two duplexes can be joined by a 2- or 3-nt linker (Fig. 3*D*). We suspect that the second duplex brought in by the crystal symmetry mimics the 5′ TBE of TER (Fig. 1*A*) (13).

Crystal Structure of a *tc*TERT Ternary Complex and Comparison with HIV RT. To capture the downstream duplex, we annealed a single RNA strand with two DNA oligos to form two 7-bp hybrid duplexes separated by a 3-nt gap (Fig. 4 *A* and *B*). Cocrystals of *tc*TERT and this gapped NL substrate were obtained in the presence of Ca^{2+} and an incoming dGTP and diffracted X-rays to 2.0 Å. In the resulting structure (*SI Appendix*, Table S1), the two linked hybrid duplexes bind to a single *tc*TERT and are nearly orthogonal to each other (Fig. 4*A*). The upstream duplex along with the incoming dGTP forms the ternary complex with *tc*TERT, and the downstream hybrid duplex, particularly the RNA strand, interacts extensively with the TRBD and finger domain. The groove between the TRBD and finger is widened compared with the ternary-complex structures without the downstream duplex (24) (*SI Appendix*, Fig. S3*B*). The TRBD is shifted in the ternary complex compared with the binary complex (*SI Appendix*, Fig. S3*C*), while the cavity for the DNA loopout is unaltered.

The incoming dGTP and Ca^{2+} ion (occupying the B site) were bound similar to *tc*TERT and HIV RT (25) (Fig. 4*C*) as essential residues in the active site are conserved between the two enzymes. A fundamental difference between them is that the active site of *tc*TERT is preformed and remains unchanged from the apo, binary, to ternary complex (9), while the finger domain of RT undergoes open-and-closed conformational changes for each dNTP incorporation (26). We find that the finger in *tc*TERT is fixed in the closed conformation by the three helix insertions (α10, α13, and α14) between the finger and palm domains on the back side of TERT (Fig. 4*C* and *SI Appendix*, Fig. S4). These three helices are conserved in all TERTs. α10 belongs to motif 3 (27), and α13 and α14 are parts of IFD (insertion in the finger domain) (28). Both motif 3 and IFD are known to be critical for the processivity of repeat addition (27, 28). The immobile finger and preformed catalytic center are probably general features of all TERTs and probably important for telomeric DNA synthesis.

Perhaps to allow dNTPs to freely diffuse in and out of the active site, the β-hairpin β5 and β6 (in the finger), which clasps the nascent replicating base pair, is 2 residues shorter than the equivalent in RT and exposes the last 2 nt (-1 and -2) in the DNA primer strand to solvent (Fig. 4*A*). The loop from the β-linker (after the palm) to CTE (K406 to N424), uniquely long in *tc*TERT, forms extensive interactions with the primer strand from -4 to -7 (Fig. 4*A*). The highly conserved T motif (aa 135 to 154, forming β3 and β4 in the TRBD), which has no equivalent in RT, reaches toward the DNA primer at the -3 and -4 positions (Fig. 4 *A*–*C*). Between the T motif and CTE, the DNA primer is held firmly at the -4 position, which explains why

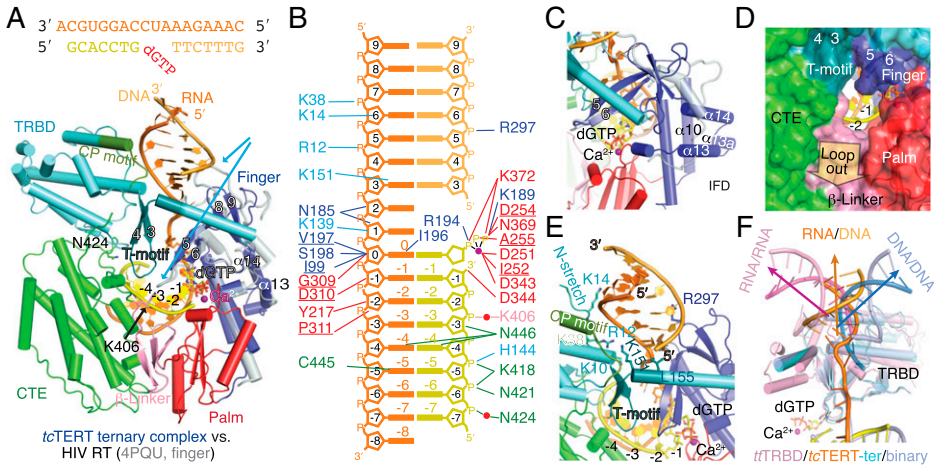

Fig. 4. Structure of the *tc*TERT–RNA/DNA–dGTP ternary complex. (*A*) The ternary-complex structure with the gapped RNA/DNA hybrid is shown in a color-coded cartoon with yellow DNA primer and orange RNA. The finger domain of HIV RT (PDB ID code 4PQU) colored in light gray is superimposed to show the deletions (β5-β6 and β7-β8, marked by blue arrows) and insertions (α10, α13, and α14) in *tc*TERT. The T motif (highlighted in teal) and CTE surround the DNA primer around the -4 position. (*B*) Diagram of *tc*TERT–RNA/DNA interactions. Protein residues are color-coded according to the domain as in *A*. (*C*) A zoomed-in view of the three-helix insertion (IFD) in *tc*TERT. Movement of the finger in *tc*TERT is blocked by the conserved IFD. (*D*) The cavity between the palm and CTE in the ring-shaped *tc*TERT can accommodate the looped-out DNA. (*E*) A zoomed-in view of dsRDH bound between the TRBD and finger in *tc*TERT. The downstream DNA is shown in light orange. (*F*) Structural comparison of *tc*TRBD–dsRDH, *tc*TRBD–DNA, and *tt*TRBD–TBE (PDB ID code 5C9H). The downstream duplexes orient differently relative to the superimposed TRBD. Moreover, the template strands, shown in a darker shade (blue DNA, orange RNA of dsRDH, and deep pink of TBE), partially overlap, but the complementary strand in each downstream duplex is positioned differently due to different rotations around the helical axis.

*tc*TERT requires a minimum of 4 bp for efficient primer extension (Fig. 2). The last 2 nt of the DNA primer (-1 and -2), however, are solvent-exposed next to the persistent cavity (Fig. 4*D*).

Mutations in the Cavity Reduce the Extension of the Looped-Out DNA Primer. As the cavity adjacent to the 3′ end of the DNA persists in *tc*TERT structures regardless of substrate-binding state, we decided to enlarge two side chains in the cavity. If the cavity accommodates the looped-out primer, reducing its size would impact on primer extension of L5,2 but not NL4 or NL8 without the loopout. P388, which is conserved in human and mouse TERT, was mutated to Arg (P338R) and, L404, which is not conserved in other TERTs, was mutated to Tyr (L404Y) (Fig. 5*A*). The mutant *tc*TERT (PR/LY) was stable and extended the normal RNA/DNA hybrids of NL4 or NL8 with similar efficiencies to wild-type (WT) enzyme (Fig. 5 *B* and *C*). However, the mutant *tc*TERT exhibited a 4.6-fold reduced k_{cat} and 1.4-fold increased K_M when extending the L5,2 looped-out primer (Fig. 5 *B* and *C*). Together with the kinetic data (Fig. 2), the mutational analysis supports the hypothesis that the structural conserved cavity in TERT accommodates the looped-out DNA.

The Downstream RNA/DNA Hybrid Mimics the RNA Duplex of TBE. In the *tc*TERT ternary-complex structure, the downstream RNA/DNA hybrid (dsRDH) is bound between the TRBD and finger domain and abuts the base of the T motif (Fig. 4 *A*

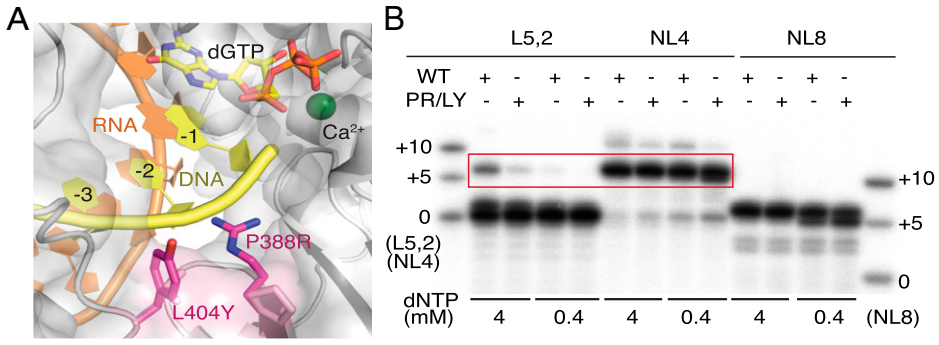

C

PR/LY	k_{cat} (min^{-1})	K_M (μM)	K_{eff} ($min^{-1}μM^{-1}$)
L5,2	$(9.1 \pm 0.5) \times 10^{-2}$	610.7 ± 101.5	1.5×10^{-4}
Relative to WT	4.6-fold ↓	1.4-fold ↑	6.4-fold ↓
NL8	19.4 ± 0.7	4.6 ± 0.4	4.2
NL4	0.7 ± 0.1	6.3 ± 1.0	0.1

Fig. 5. Smaller cavity impedes the looped-out DNA extension. (*A*) The structural model of P388R and L404Y mutations in *tc*TERT (PR/LY). WT protein is shown as a gray cartoon and semitransparent molecular surface. Side chains of Arg and Tyr, which reduce the cavity size, and original Pro and Leu are shown as magenta and pink sticks, respectively. (*B*) Extension of the looped-out L5,2 and normal DNA primers (NL4 and NL8) by WT and PR/LY in the presence of 0.4 or 4 mM dNTP. Markers of DNA substrate (0) and products (+5 and +10) of different primers are shown on either side of the gel. (*C*) Kinetic measurements of PR/LY mutant *tc*TERT on looped-out and normal DNA primers. Changes relative to the WT enzyme are indicated for L5,2.

and *B*). The CP motif (aa 35 to 45) conserved among TERTs and the N-terminal extended region of *tc*TERT (K10, R12, K14, and K17) form a positively charged surface that cradles six phosphates of the RNA strand (Fig. 4*E*). The complementary DNA strand in dsRDH formed terminal base stacking with hydrophobic residues in the T motif (I155) and sparse interactions with the finger (R297) (Fig. 4*E*). *tc*TERT can bind the downstream duplex because the pair of β-strands (β8 and β9) in the finger domain are truncated by 9 residues compared with HIV RT, which accommodates a single-stranded template only (Fig. 4*A*). The truncation of β8 and β9 is also observed in human and *Tetrahymena* TERT (4, 16).

The orientation of the downstream duplex (dsRDH) appears to be flexible and is rotated by 30° compared with the DNA duplex bound in trans in the NL binary-complex structure (Fig. 4*F*). TBE of *Tetrahymena thermophila* TER captured in the crystal structure of the *tt*TRBD (13) and in the intact telomerase cryo-EM structure (3) reveals another orientation. When the TRBDs are superimposed (Fig. 4*F* and *SI Appendix*, Fig. S5) TBE and dsRDH occupy a similar space, and the RNA-template strands even partially overlap, but TBE is rotated by 40° compared with dsRDH (Fig. 4*F*). Such flexible interactions between TBE and TERT may be species-dependent or reflect the mobility of TBE during telomeric repeat synthesis.

The Downstream RNA Duplex Enhances *tc*TERT Catalytic Activity. The duplex downstream of the template region (dsRDH or TBE) is near the catalytic site in both *tc*TERT (Fig. 4*A*) and *Tetrahymena* telomerase (3). To determine whether the downstream RNA duplex alters the catalytic activity of *tc*TERT, we synthesized several RNA template/DNA primer pairs with a downstream 8-bp RNA duplex, and the template/primer pair contained either a normal hybrid (RDR) or a looped-out DNA primer (LRDR) (Fig. 6*A*). The single-stranded RNA gap between the template/primer pair and RNA duplex was varied from 1 to 5 nt (1g_ to 5g_RDR or LRDR) (Fig. 6*A*), which mimics the change in nucleotide number between the DNA primer end and TBE in each cycle of telomeric repeat synthesis (Fig. 1*A*). The efficiency of single-nucleotide incorporation by *tc*TERT in these 10 substrate variations was compared with those without the downstream RNA duplex (Fig. 6).

With a normal template/primer pair, the addition of a downstream duplex after a gap of 2 nt or larger increased k_{cat}, decreased K_M, and thus enhanced K_{eff} by ~5-fold (Fig. 6*B* and *SI Appendix*, Fig. S6). The RNA of varied length (1 to 4 nt) between the template base and TBE appears to be looped-out in the back of the finger domain as observed in the telomerase structures (*SI Appendix*, Fig. S1 *E* and *F*) (4, 16). With the gap size of 1 nt, which left no single-stranded region during nucleotide incorporation, the downstream RNA duplex led to slightly reduced k_{cat}/K_M (Fig. 6*B*). In parallel, the presence of downstream RNA after a 2-nt gap also increased the catalytic activity of the looped-out primers, 2.5-fold with the gap of 2 nt and ~1.5-fold with 3 to 5 nt (Fig. 6*C* and *SI Appendix*, Fig. S5). The activity of 1g_LRDR was also worse than without a downstream RNA duplex (Fig. 6*C*). The native TBE duplex in TER is at least 3 nt away from the end of the RNA template (http://telomerase.asu.edu/sequences_tr.html). We further checked the primer extension of NL4, which formed the shortest hybrid (4 bp) for primer extension, and found the downstream dsRNA enhances catalytic efficiency by 8-fold, more significantly than the 8-bp template/primer pair (Fig. 6*D*). We suspect that TBE or a TBE-like duplex not only marks the RNA-template

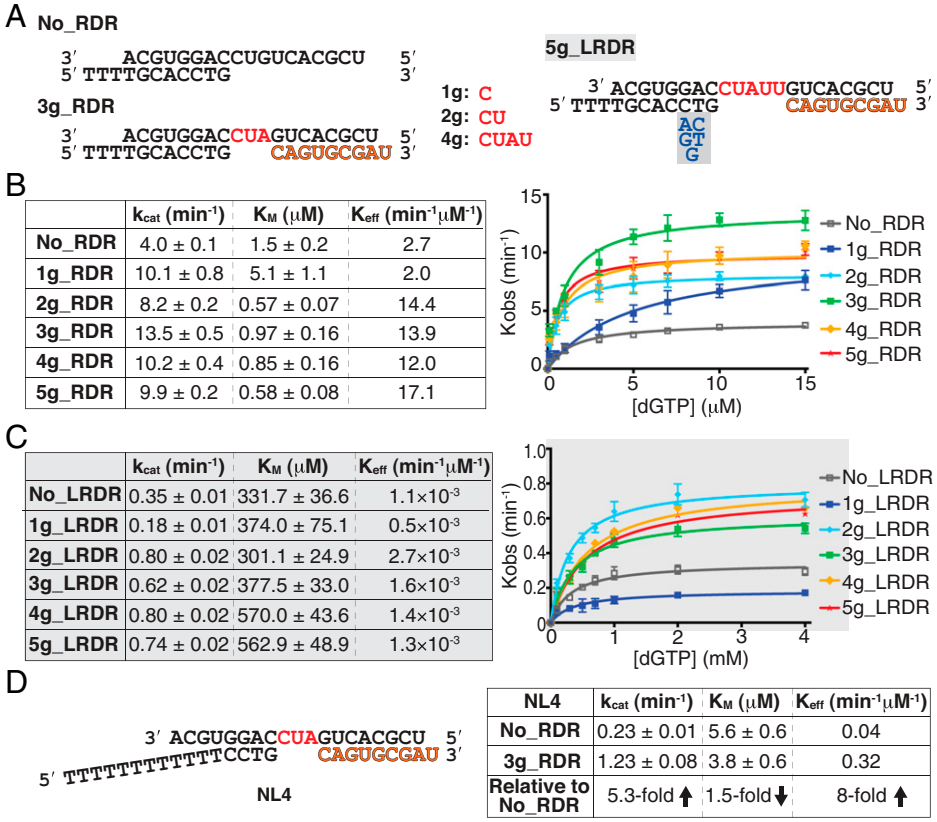

	k_{cat} (min^{-1})	K_M (μM)	K_{eff} (min^{-1}μM^{-1})
No_RDR	4.0 ± 0.1	1.5 ± 0.2	2.7
1g_RDR	10.1 ± 0.8	5.1 ± 1.1	2.0
2g_RDR	8.2 ± 0.2	0.57 ± 0.07	14.4
3g_RDR	13.5 ± 0.5	0.97 ± 0.16	13.9
4g_RDR	10.2 ± 0.4	0.85 ± 0.16	12.0
5g_RDR	9.9 ± 0.2	0.58 ± 0.08	17.1

	k_{cat} (min^{-1})	K_M (μM)	K_{eff} (min^{-1}μM^{-1})
No_LRDR	0.35 ± 0.01	331.7 ± 36.6	1.1×10^{-3}
1g_LRDR	0.18 ± 0.01	374.0 ± 75.1	0.5×10^{-3}
2g_LRDR	0.80 ± 0.02	301.1 ± 24.9	2.7×10^{-3}
3g_LRDR	0.62 ± 0.02	377.5 ± 33.0	1.6×10^{-3}
4g_LRDR	0.80 ± 0.02	570.0 ± 43.6	1.4×10^{-3}
5g_LRDR	0.74 ± 0.02	562.9 ± 48.9	1.3×10^{-3}

NL4	k_{cat} (min^{-1})	K_M (μM)	K_{eff} (min^{-1}μM^{-1})
No_RDR	0.23 ± 0.01	5.6 ± 0.6	0.04
3g_RDR	1.23 ± 0.08	3.8 ± 0.6	0.32
Relative to No_RDR	5.3-fold ↑	1.5-fold ↓	8-fold ↑

Fig. 6. Downstream RNA duplex enhances *tc*TERT catalytic activity. (*A*) RNA template and DNA primer pairs with or without a loopout followed by a downstream RNA duplex after a 1- to 5-nt gap (LRDR and RDR). Three of the 12 substrates tested are shown, and the gap sequences are illustrated if not included in the examples. (*B* and *C*) Summary of the kinetic measurements and plots of experimental data of nucleotide incorporation by *tc*TERT on normal template/primer pairs (RDR; *B*) and the looped-out substrate (LRDR; *C*). (*D*) The downstream dsRNA enhances the NL4 extension in a 4-bp RNA/DNA hybrid by eightfold.

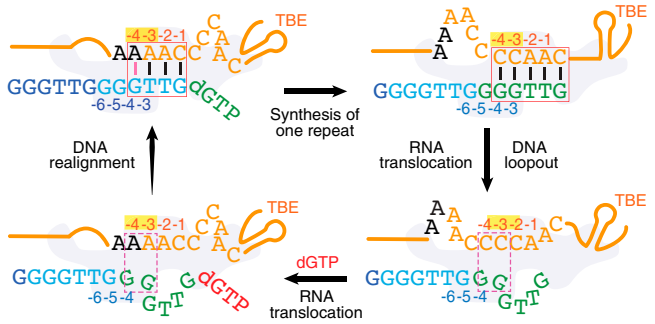

Fig. 7. Revised model of telomeric repeat synthesis. The *Tetrahymena* sequence is used as an example. The "accordion" effects (looping out and straightening) surrounding the RNA template (31) in one repeat addition are shown in the first two panels. In the third panel, while base-paired at the -3 and -4 positions, the RNA template translocates with the DNA, resulting in a DNA loopout in the cavity at the -2 and -3 positions. With the DNA straddling the bottleneck outlined in the dashed purple box, the RNA template completes translocation as shown in the fourth panel. After the DNA primer realigns with the RNA template for the next round of repeat addition, the diagram returns to a new beginning (indicated by the tapered arrowhead) with the green primer and red dGTP replacing the blue primer and green dGTP. TERT is diagrammed as a gray blob in the background. The 4- to 5-bp hybrid duplex (outlined by the solid red box) may contain both Watson–Crick and Hoogsteen pairs, indicated by black and pink lines.

boundary but also enhances the telomerase activity by stabilizing the RNA template.

A Revised Model of RNA-Template Translocation. The sequence- and position-dependent binding and extension of L5,2 by *tc*TERT (Fig. 2) and the reduced extension capacity by the smaller cavity size (Fig. 5) provide experimental support for the DNA looped-out model (Fig. 1*B*). Our crystal structures of *tc*TERT binary and ternary complexes highlight the conserved central cavity, which results in few interactions with the -2 and -3 primer strands and thus very inefficient extension of NL3. As observed in the crystal structures of *tc*TERT, the RNA template from the nascent base pair to the -4 position is also snugly bound by human and *Tetrahymena* TERT (3, 4). In addition, the TRBD and CTE domain form a structurally conserved "bottleneck" surrounding the -3 to -4 base pairs of the hybrid. The 20-Å diameter of the bottleneck holds the RNA/DNA hybrid together, which is probably why the 4-bp NL4 is much more efficiently extended than NL3. But the bottleneck prevents unpairing of the RNA and DNA hybrid and makes the looped-out model appealing.

Previous analyses suggest that the hybrid between the template RNA and telomeric DNA may be limited to 7 bp by telomerase (29, 30). In the cryo-EM structures of human and *Tetrahymena* telomerase–DNA complexes, the hybrid consists of 4 to 5 bp only (4, 16). Such a short hybrid duplex reduces the DNA synthesis efficiency (Fig. 2). As shown in Fig. 6, other interactions between TER and TERT can enhance the TERT activity, for example, the downstream RNA duplex (TBE) bound between the TRBD and finger (Fig. 4) and the upstream RNA bound between the thumb and TEN/TRAP (of IFD) (3, 4) (*SI Appendix*, Fig. S1). The 4- to 5-bp short RNA/DNA hybrid, however, makes separation of the RNA and DNA strands easier in the popular model (Fig. 1*A*) and looping out an entire telomeric repeat (Fig. 1*B*) unnecessary and unlikely. Instead, looping out 2 or 3 nt in the DNA primer may be sufficient to separate the RNA/DNA hybrid duplex and allow the RNA template to translocate between cycles of repeat synthesis (Fig. 7).

For human and *Tetrahymena* telomerase, we suggest that 2 bp at the -3 and -4 positions are held together until they are translocated through the bottleneck. As the 3′ primer end is held by the active site as observed in all DNA polymerases including RT and TERT, the translocated DNA is likely looped-out in the conserved cavity. The following DNA backbone may straddle the bottleneck with the bases tilted to provide space for the RNA template to slide through (Fig. 7). With limited interactions between TERT and the DNA primer, the looped-out DNA can straighten, realign, and reanneal with the translocated RNA template.

Conclusions

The active site of TERT is rigid, but the porous structure of TERT allows TER surrounding the template region to loop out as evidenced in fluorescence resonance energy transfer measurement and cryo-EM structures (4, 16, 31, 32) (Fig. 7). The extension of the looped-out DNA primer (L5,2) by *tc*TERT suggests that the conserved central cavity may be essential and necessary to accommodate the primer loopout and facilitate RNA-template translocation. Our structural and biochemical characterization of the RNA duplex downstream of the template region reveals that TBE and TBE-like elements can enhance the telomerase activity. Based on these findings and the recently reported cryo-EM structures of human and *Tetrahymena* telomerases, we propose a revised mechanism for repeat addition processivity (Fig. 7), which combines the features of two earlier models (Fig. 1) and can be verified by mutagenic studies of human and *Tetrahymena* TERT.

Data Availability. The structures and structure factors reported in this article have been deposited in the Protein Data Bank (ID codes 7KQM and 7KQN).

All study data are included in the article and/or *SI Appendix*.

ACKNOWLEDGMENTS. We thank Drs. R. Craigie, M. Gellert, and J. L. Chen for critical reading of the manuscript, and are grateful for funding by NIH Intramural Programs DK036144 and DK036146.

1. E. H. Blackburn, Structure and function of telomeres. *Nature* **350**, 569–573 (1991).
2. E. H. Blackburn, K. Collins, Telomerase: An RNP enzyme synthesizes DNA. *Cold Spring Harb. Perspect. Biol.* **3**, a003558 (2011).
3. J. Jiang *et al.*, Structure of telomerase with telomeric DNA. *Cell* **173**, 1179–1190.e13 (2018).
4. G. E. Ghanim *et al.*, Structure of human telomerase holoenzyme with bound telomeric DNA. *Nature* **593**, 449–453 (2021).
5. T. M. Nakamura *et al.*, Telomerase catalytic subunit homologs from fission yeast and human. *Science* **277**, 955–959 (1997).
6. R. A. Wu, H. E. Upton, J. M. Vogan, K. Collins, Telomerase mechanism of telomere synthesis. *Annu. Rev. Biochem.* **86**, 439–460 (2017).
7. C. D. Hardy, C. S. Schultz, K. Collins, Requirements for the dGTP-dependent repeat addition processivity of recombinant *Tetrahymena* telomerase. *J. Biol. Chem.* **276**, 4863–4871 (2001).
8. W. Yang, Y. S. Lee, A DNA-hairpin model for repeat-addition processivity in telomere synthesis. *Nat. Struct. Mol. Biol.* **22**, 844–847 (2015).
9. M. Mitchell, A. Gillis, M. Futahashi, H. Fujiwara, E. Skordalakes, Structural basis for telomerase catalytic subunit TERT binding to RNA template and telomeric DNA. *Nat. Struct. Mol. Biol.* **17**, 513–518 (2010).
10. J. Lingner *et al.*, Reverse transcriptase motifs in the catalytic subunit of telomerase. *Science* **276**, 561–567 (1997).
11. A. J. Gillis, A. P. Schuller, E. Skordalakes, Structure of the *Tribolium castaneum* telomerase catalytic subunit TERT. *Nature* **455**, 633–637 (2008).
12. S. Rouda, E. Skordalakes, Structure of the RNA-binding domain of telomerase: Implications for RNA recognition and binding. *Structure* **15**, 1403–1412 (2007).
13. L. I. Jansson *et al.*, Structural basis of template-boundary definition in *Tetrahymena* telomerase. *Nat. Struct. Mol. Biol.* **22**, 883–888 (2015).
14. A. R. Robart, K. Collins, Human telomerase domain interactions capture DNA for TEN domain-dependent processive elongation. *Mol. Cell* **42**, 308–318 (2011).
15. B. Min, K. Collins, An RPA-related sequence-specific DNA-binding subunit of telomerase holoenzyme is required for elongation processivity and telomere maintenance. *Mol. Cell* **36**, 609–619 (2009).
16. Y. He *et al.*, Structures of telomerase at several steps of telomere repeat synthesis. *Nature* **593**, 454–459 (2021).
17. M. Osanai, K. K. Kojima, R. Futahashi, S. Yaguchi, H. Fujiwara, Identification and characterization of the telomerase reverse transcriptase of *Bombyx mori* (silkworm) and *Tribolium castaneum* (flour beetle). *Gene* **376**, 281–289 (2006).

18. S. Doublié, M. R. Sawaya, T. Ellenberger, An open and closed case for all polymerases. *Structure* **7**, R31–R35 (1999).
19. Y. S. Lee, Y. Gao, W. Yang, How a homolog of high-fidelity replicases conducts mutagenic DNA synthesis. *Nat. Struct. Mol. Biol.* **22**, 298–303 (2015).
20. J. M. Clark, Novel non-templated nucleotide addition reactions catalyzed by procaryotic and eucaryotic DNA polymerases. *Nucleic Acids Res.* **16**, 9677–9686 (1988).
21. M. P. Golinelli, S. H. Hughes, Nontemplated nucleotide addition by HIV-1 reverse transcriptase. *Biochemistry* **41**, 5894–5906 (2002).
22. F. Wang, W. Yang, Structural insight into translesion synthesis by DNA Pol II. *Cell* **139**, 1279–1289 (2009).
23. C. Bryan *et al.*, Structural basis of telomerase inhibition by the highly specific BIBR1532. *Structure* **23**, 1934–1942 (2015).
24. M. A. Schaich *et al.*, Mechanisms of nucleotide selection by telomerase. *eLife* **9**, e55438 (2020).
25. K. Das, S. E. Martinez, R. P. Bandwar, E. Arnold, Structures of HIV-1 RT-RNA/DNA ternary complexes with dATP and nevirapine reveal conformational flexibility of RNA/DNA: Insights into requirements for RNase H cleavage. *Nucleic Acids Res.* **42**, 8125–8137 (2014).
26. W. Yang, Y. Gao, Translesion and repair DNA polymerases: Diverse structure and mechanism. *Annu. Rev. Biochem.* **87**, 239–261 (2018).
27. M. Xie, J. D. Podlevsky, X. Qi, C. J. Bley, J. J. Chen, A novel motif in telomerase reverse transcriptase regulates telomere repeat addition rate and processivity. *Nucleic Acids Res.* **38**, 1982–1996 (2010).
28. N. F. Lue, Y. C. Lin, I. S. Mian, A conserved telomerase motif within the catalytic domain of telomerase reverse transcriptase is specifically required for repeat addition processivity. *Mol. Cell. Biol.* **23**, 8440–8449 (2003).
29. K. Förstemann, J. Lingner, Telomerase limits the extent of base pairing between template RNA and telomeric DNA. *EMBO Rep.* **6**, 361–366 (2005).
30. P. W. Hammond, T. R. Cech, *Euplotes* telomerase: Evidence for limited base-pairing during primer elongation and dGTP as an effector of translocation. *Biochemistry* **37**, 5162–5172 (1998).
31. A. J. Berman, B. M. Akiyama, M. D. Stone, T. R. Cech, The RNA accordion model for template positioning by telomerase RNA during telomeric DNA synthesis. *Nat. Struct. Mol. Biol.* **18**, 1371–1375 (2011).
32. J. W. Parks, M. D. Stone, Coordinated DNA dynamics during the human telomerase catalytic cycle. *Nat. Commun.* **5**, 4146 (2014).